Journal of Catalysis 280 (2011) 77–88

Contents lists available at ScienceDirect

Journal of Catalysis

journal homepage: www.elsevier.com/locate/jcat

Influence of Ni species on the structural evolution of Cu/SiO_2 catalyst for the chemoselective hydrogenation of dimethyl oxalate

Anyuan Yin, Chao Wen, Xiaoyang Guo, Wei-Lin Dai *, Kangnian Fan

Department of Chemistry and Shanghai Key Laboratory of Molecular Catalysis and Innovative Materials, Fudan University, Shanghai 200433, People's Republic of China

ARTICLE INFO

Article history:
Received 5 January 2011
Revised 2 March 2011
Accepted 7 March 2011
Available online 13 April 2011

Keywords:
CuNi/HMS
Dimethyl oxalate
Ethylene glycol
Methyl glycolate
Hydrogenation

ABSTRACT

A novel family of heterogeneous $Cu–Ni/SiO_2$ catalysts with appropriate metal ratios displayed outstanding selectivity to methyl glycolate (96%) and to ethylene glycol (98%) in the chemoselective gas-phase hydrogenation of dimethyloxalate. The chemical states of nickel species were found to have a strong influence on the structural evolution of the catalysts and correspondent catalytic behaviors. The selectivity to the two products could be tuned by modulating the chemical states of nickel species. It is shown that oxidative nickel species are helpful in improving the dispersion of copper species because of the enrichment of copper on the surface of the nickel species, thus enhancing the catalytic activity and selectivity to ethylene glycol. The selectivity to methyl glycolate could be greatly improved by the Cu–Ni bimetallic catalyst. An 83% yield of methyl glycolate and a 98% yield of ethylene glycol could be obtained over the bimetallic Cu–Ni catalyst and the NiO-modified catalyst, respectively.

1. Introduction

Because of their superior catalytic performance, bimetallic catalysts have wide applications in catalytic reforming [1], selective hydrogenation [2], and selective alcohol oxidation [3]. The introduction of a second metal is an important approach to tailoring the electronic and geometric structures of the catalysts to enhance their activity and modulate their selectivities for products [4–8]. Recent investigations have demonstrated that the structure, chemical composition, and surface chemical state of bimetallic catalysts play a critical role in determining their catalytic properties. By combining both experimental studies and theoretical calculations, many fundamental investigations have been carried out in an effort to correlate the electronic properties of bimetallic surfaces with chemical reactivities [9–12]. Establishing the connection between the catalytic activity and selectivity of a catalyst and its physical and electronic structure is crucial for the design of new catalysts.

Great efforts have been made to improve the catalytic activity of Cu-based catalysts by introducing a second metal, such as Ag [13], Au [14], and Pd [15], most of which are noble metals. The chemical state of Cu was the same as in the solely Cu-based catalyst due to the chemical stability of the noble metals. It is found that Ni and Cu both have *fcc* structures with lattice parameters 3.51 and 3.61 Å, respectively. They can form a continuous solid solution of cupronickel binary alloys crystallized in a cubic close packed lattice. Ni-based bimetallic catalysts containing Cu exhibit significantly different catalytic activity and selectivity than Ni monometallic catalysts [16–20]. However, some controversial results for Ni–Cu alloy catalysts have been reported. The water–gas shift activity in the presence of CO_2 [17] and the catalytic hydrogenation activity for ethylene hydrogenation [18,19] could be greatly enhanced by the introduction of Cu into the Ni catalyst. The addition of Cu to Ni/Al_2O_3 also increases the selectivity to 1-butene [16]. Also, the addition of Cu favors CO formation in CO_2 hydrogenation [20] and could dramatically enhance the generation of carbon fibers from the decomposition of hydrocarbons [21]. Changes in the catalytic performance induced by adding Cu to Ni can be caused by changes in the electronic properties of the homogeneous alloy particle, the formation of active surface structure, or the preferential segregation of one metal to the surface, or by a combination of all these effects [16–21]. However, the addition of copper to nickel foil significantly reduced the catalytic activity for styrene hydrogenation and hydrogenolysis of ethane to methane [22,23]. The decrease in catalytic activity was explained by changes in the electronic properties of nickel upon the addition of copper [22]. The original ability of the bimetallic catalyst to influence the catalytic behavior still faces a great challenge to elucidate. Effects of the introduction of Cu into the nickel catalyst have been extensively studied during the past few years; however, the influences of the modification with Ni on the copper catalyst have been less considered. In the present work, systematic investigations were carried out to elucidate the effects of Ni on the Cu based catalysts.

Chemoselective gas-phase hydrogenation of dimethyl oxalate (DMO) to corresponding methyl glycolate (MG) and ethylene gly-

* Corresponding author. Fax: +86 21 55664678.
E-mail address: wldai@fudan.edu.cn (W.-L. Dai).

0021-9517/$ - see front matter © 2011 Elsevier Inc. All rights reserved.
doi:10.1016/j.jcat.2011.03.006

col (EG) has great academic and industrial significance owing to their highly added value as building blocks [24]. In this context, catalytic methods leading to high-quality grade MG and EG via the design of the catalysts are particularly attractive for applications in the polymer and fine chemical industries. Previous study showed that higher yields of MG and EG could be obtained by controlling the reaction temperature via the versatile Ag/SiO_2 catalyst [25]. However, the large amount of noble metal used limited its further application in industry. Developing a much cheaper and highly efficient catalyst is therefore economically and environmentally benign.

It is commonly accepted that the catalyst surface plays the main role in the catalytic reactions and the composition of the surface may not be the same as that of the bulk due to the differences in the volatility of nickel and copper [26]. The *d*-band vacancies theory was suggested to account for the binding energy changes of nickel and copper upon alloying in X-ray photoelectron spectroscopy (XPS) [27]. Moreover, it was recognized that, in addition to *d*-band vacancies, other factors, such as surface composition, must also be taken into account when the properties of nickel–copper catalysts are investigated. Chemoselective hydrogenation of DMO is a two-step continuous hydrogenation reaction, and EG could be obtained by hydrogenation of DMO via MG. From a thermodynamic viewpoint, it is easy to get EG due to the much larger equilibrium constant than that of the first-step hydrogenation reaction. Therefore, how to control the product distributions via designing and structuring the catalyst was a great challenge. In previous studies [28–33], Cu/HMS and Cu/Al–HMS catalysts applied in the hydrogenation of DMO were systematically investigated in relation to the optimization of the catalyst preparation parameters and preparation methods and the active center discussion. A high yield of EG could be obtained under optimized conditions. Introduction of nickel species into the Cu/SiO_2 catalyst would help not only to understand deeply the origin of the catalyst itself, but also to supply a reference for catalysis in the hydrogenation of ester.

In the present work, we report a novel family of ternary Cu–Ni–Si catalysts with outstanding MG and EG selectivity in the gas-phase hydrogenation of DMO, obtained by adjusting the surface chemical state of nickel species. The design comprised the incorporation of components with complementary functions into the heterogeneous catalyst: copper as the basic hydrogenation metal, optimized amounts of nickel as a promoter to increase the dispersion of copper species, and silica as the support of exposed copper and nickel sites.

2. Experimental

2.1. Catalyst preparation

2.1.1. HMS

Mesoporous siliceous HMS was prepared according to a well-established procedure delineated by Tanev and Pinnavaia [34] using tetraethyl orthosilicate (TEOS) as silica source and dodecylamine (DDA) as template agent. Typically, the HMS materials were prepared by dissolving 5.04 g of DDA in 53.33 g of deionized H_2O and 39.42 g of ethanol under vigorous stirring before adding 21.39 g of TEOS dropwise. The solution mixture was then stirred at 313 K for 0.5 h. The resulting gel was aged for 18 h at ambient temperature to afford the crystalline templated product. After that, the resulting solid was recovered by filtration, washed with deionized water, and dried at 373 K, followed by calcination at 923 K for 3 h.

2.1.2. CuxNi/HMS

Nickel-modified Cu/HMS catalysts containing 20 wt% copper loading were prepared by the ammonia evaporation method (AE). In a typical procedure, 7.625 g of $Cu(NO_3)_2{\cdot}3H_2O$ and a certain amount of $Ni(NO_3)_2{\cdot}6H_2O$ were dissolved in 172 ml of deionized water. Then 23 ml of 28% ammonia aqueous solution was added and stirred for 0.5 h at 333 K. A certain amount of HMS was added to the above solution and stirred for another 4 h. The initial pH of the suspension was 11–12. The suspension was then preheated at 363 K to evaporate ammonia and decrease of pH and consequently deposit copper and nickel species on silica. When the pH value of the suspension decreased to 7–8, the evaporation process was terminated. The filtrate was washed with deionized water and dried at 393 K overnight, followed by calcination at 723 K for 4 h. The catalyst precursor was denoted as CuxNi/HMS, where x represents NiO loading. The catalysts reduced under 5% H_2/Ar flow at 543 K for 4 h were correspondingly denoted as CuxNi/HMS-re. For example, Cu3Ni/HMS is composed of 20 wt% Cu, 3 wt% NiO, and 77 wt% HMS.

For comparison, the Cu/HMS catalyst with 20 wt% Cu loading, denoted as 20Cu/HMS, and the Ni/HMS catalyst with 3 wt% NiO, denoted as 3Ni/HMS, were also prepared by the AE method.

2.1.3. Bimetallic Cu_xNi_y/HMS

The bimetallic CuNi/HMS catalyst precursors were prepared by a chemical reduction deposition method involving the reduction of two precursors with KBH_4 under Ar flow. HMS was impregnated with the desired amount of aqueous solution of $Cu(AC)_2{\cdot}3H_2O$ and $Ni(AC)_2{\cdot}6H_2O$; then KBH_4 solution (0.05 M) was added dropwise to the mixture. The metal-loaded powder was then dried in an oven under Ar at 383 K for 16 h, and calcined at 723 K for 4 h. Finally, the sample was reduced at 673 K with 5% H_2/Ar for 4 h and was denoted as Cu_xNi_y/HMS, where *x* and *y* stand for the mole ratio of Cu/Ni. The total bimetal loading was controlled at 5 wt%.

2.2. Catalyst characterization

The BET surface area (S_{BET}) was measured using N_2 physisorption at 77 K on a Micromeritics Tristar 3000 apparatus. The pore size distributions were obtained from the desorption isotherm branch of the nitrogen isotherms using Barrett–Joyner–Halenda (BJH) method. The powdered X-ray diffraction (XRD) patterns were collected on a Bruker D8 Advance X-ray diffractometer using nickel-filtered Cu Kα radiation (λ = 0.15418 nm) with a scanning angle (2θ) of 10°–90°, a scanning speed of 2° min^{-1}, and a voltage and current of 40 kV and 40 mA, respectively. Elemental analysis of Cu and Ni loading was performed using ion-coupled plasma (ICP) atomic emission spectroscopy on a Thermo Electron IRIS Intrepid II XSP spectrometer. Transmission electron microscopy (TEM) and energy-dispersive X-ray spectrometry microanalysis (EDX) were performed on a JEOL JEM2011 instrument.

Temperature-programmed reduction (TPR) profiles were obtained on a Tianjin XQ TP5080 autoadsorption apparatus. A 50-mg sample of the calcined catalyst was outgassed at 473 K under Ar flow for 2 h. After the sample was cooled to room temperature under Ar flow, the in-line gas was switched to 5% H_2/Ar, and the sample was heated to 1073 K at a ramping rate of 10 K min^{-1}. The H_2 consumption was monitored by a TCD detector. The metallic Cu surface area was measured by decomposition of N_2O at 363 K using a pulsed method, with N_2 as the carrier gas [35]. The consumption of N_2O was also detected by a TCD detector. The specific area of metallic copper was calculated from the total amount of N_2O consumption with 1.46×10^{19} copper atoms per m^2. XPS experiments were carried out with a Perkin–Elmer PHI 5000C ESCA system equipped with a hemispherical electron energy analyzer. The Mg Kα ($h\nu$ = 1253.6 eV) anode was operated at 14 kV and 20 mA. The carbonaceous C1*s* line (284.6 eV) was used as a reference to calibrate the binding energies (BEs).

2.3. Activity measurements

The gas-phase hydrogenation of DMO was performed in a continuous-flow fixed-bed microreactor, which has been described in detail elsewhere [28]. Prior to the catalytic measurement, the catalysts were activated by in situ reduction with 5% H_2/Ar. In this study the following reaction conditions were used: H_2/DMO molar ratio 100, temperature (T) 473 K, total pressure (P) 2.5 MPa, and room-temperature liquid hourly space velocity (LHSV) of DMO ranged from 0.2 to 1.8 h^{-1}.

To eliminate internal diffusion, catalysts with different grain diameters were used to evaluate the effect of diffusion. The experimental results showed that the conversion of DMO did not vary with the change of grain diameter, which indicated that no diffusion effect could happen when the grain diameter of the catalyst was less than 20 mesh. Also, since the H_2/DMO molar ratio was about 100, and there was 85% methanol in the feed flow, no external diffusion effect was observed.

The heat transport effect was also considered. The total heat of reaction of the two-step hydrogenation is −37.41 kJ/mol at 478 K. Although the heat of reaction is large, the adiabatic temperature rise is rather low at very high H_2/ester ratios (100–120). In the integral reactor of our lab, the amounts of catalyst are 1–5 g, and the horizontal and vertical temperature difference is within ±0.5 K. By regulating the temperature of the fixed-bed layer via the temperature-controlled instrument, the reaction heat could be eliminated quickly in the equalizing zone and the maximum temperature difference was no more than 1.0 K.

3. Results and discussion

3.1. Characterization of Ni modified samples

3.1.1. Structural evolution and textural properties of the catalysts

The physicochemical properties of the synthesized CuxNi/HMS catalysts are summarized in Table 1. Compared with the HMS support, the S_{BET} of the 3Ni/HMS sample decreased more obviously than that of the Cu/HMS sample with 20 wt% copper loading, although the nickel loading was far lower than the copper loading, which indicated that the effect of nickel on the textural structure was greater than that of copper. This phenomenon was more pronounced on the nickel-modified Cu/HMS samples. However, the S_{BET} of the samples rose from 226 to 361 $m^2\ g^{-1}$ as the amount of nickel increased from 1 to 5 wt%, suggesting that nickel silicate or copper silicate was generated during the synthesis procedure. The N_2 adsorption–desorption isotherms and BJH pore size distributions of the calcined catalysts are presented in Fig. 1. All the samples exhibited Langmuir type IV isotherms with an H1-type hysteresis loop, corresponding to a typical large-pore mesoporous material with a 1D cylindrical channel. Capillary condensation of nitrogen with uniform mesopores occurred, causing a sudden steep increase in nitrogen uptake in the characteristic relative pressure (P/P_0) range of 0.3–0.5 for all the samples investigated, implying a typical mesoporous structure with uniform pore diameter. Because HMS exhibited a uniform hexagonal array of mesopores connected by smaller micropores, the broad hysteresis loop in the isotherms was an indication of long mesopores, which limited the emptying and filling of the accessible volume.

It is worth noting that all the physisorption curves of the nickel-containing samples exhibited the same shape, except for the Cu/HMS sample, which suggests the effect of nickel on the textural structure of the catalysts. The pore size distribution curve calculated from the desorption branch of the isotherms (Fig. 1B) exhibited a bimodal distribution at 2.5 and 3.8 nm. Compared with the Cu/HMS sample, another kind of larger pore was generated, indicating that redissolution and reprecipitation might happen during the synthetic procedure. To address this issue, an experiment exposing the support to the same pH conditions during the catalyst synthesis was carried out and N_2-sorption characterization was also conducted. The BET surface area, average pore volume, and average pore diameter are also listed in Table 1. It is interesting to find that a redissolution and reprecipitation process has happened during the synthesis procedure, and the BET surface area and average pore volume decreased from 970 to 220 $m^2\ g^{-1}$ and from 0.90 to 0.53 $cm^3\ g^{-1}$, respectively, while the average pore diameter increased from the original 3.88 to 9.05 nm. In addition, for the nickel-modified Cu/HMS samples, the main pore diameter was 3.8 nm (not the original 2.5 nm), indicating that the textural structure of the catalyst was determined not only by the copper species but also by the nickel species. The 3Ni/HMS catalyst showed, besides the main pores at 3.8 nm, the presence of smaller pores at about 2.5 nm that probably corresponded to the porosity provided by the laminar structure of nickel phyllosilicate, which was also observed in Ni/SBA-15 catalyst prepared by the deposition–precipitation method [36]. In line with the above assumption, the hysteresis of the nitrogen adsorption isotherm is enlarged due to the porosity contribution of the lamellar hydrosilicates, which also contributes to the surface area and average pore diameter val-

Table 1
Physicochemical properties of as-synthesized CuxNi/HMS catalysts.

Catalyst	Ni/Cu[a] (mol/mol)	S_{BET} ($m^2\ g^{-1}$)	V_{pore} ($cm^3\ g^{-1}$)	D_{pore} (nm)	S_{Cu}[b] ($m^2\ g_{Catal}^{-1}$)	TOF[c] (h^{-1})	S_{EG}[d] (%)
HMS	–	970	0.90	2.88	–	–	–
HMS[e]	–	220	0.53	9.05			
Cu/HMS	0	556	0.36	2.20	11.6	2.6	21
Cu1Ni/HMS	0.054	226	0.39	2.76	13.7	8.6	28
Cu3Ni/HMS	0.162	296	0.38	3.93	21.6	19.7	35
Cu5Ni/HMS	0.270	361	0.46	4.26	14.6	2.4	18
Cu7Ni/HMS	0.378	337	0.29	4.39	8.2	2.2	17
3Ni/HMS	–	482	0.84	6.27	–	–	–
Cu/HMS[f]	–	556	0.36	2.20	0.5	0.2	–
Cu/HMS[g]	–	239	0.57	7.20	9.3	1.9	–
Cu/Al–HMS[h]	–	1005	1.30	4.60	13.7	38.8	–

[a] Determined by ICP–AES analysis.
[b] Cu metal surface area determined by N_2O titration method.
[c] TOF (DMO molecular reacted per mol surface Cu per hour) at LHSV = 1.7 h^{-1} and 473 K.
[d] EG selectivities of different Ni loading catalysts at the 50% DMO conversion.
[e] Exposing the HMS to the same conditions encountered during the catalyst synthesis.
[f] Ref. [28].
[g] Ref. [31].
[h] Ref. [33].

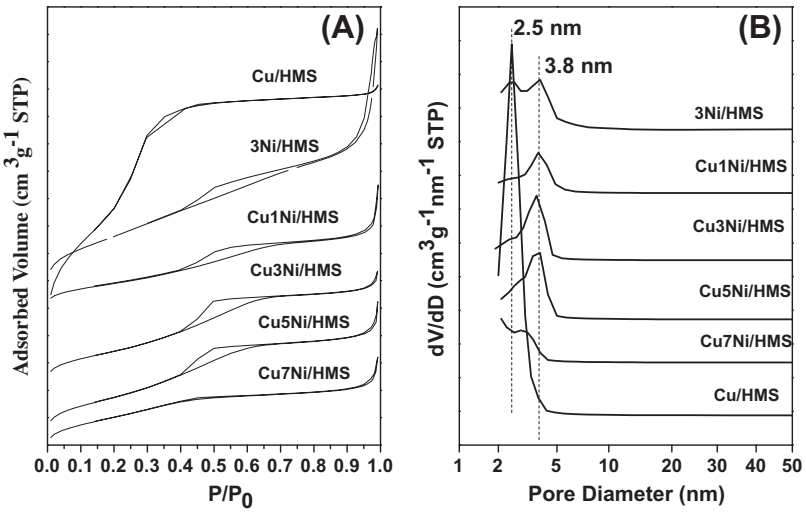

Fig. 1. (A) N_2 adsorption–desorption isotherms and (B) BJH pore size distribution of the calcined catalysts.

ues. A concrete proportion of nickel phyllosilicate could be obtained by deconvolution of the TPR profile of 3Ni/HMS sample.

To understand the nature of the copper and nickel species after calcination and reduction at 543 K for 4 h under 5% H_2/Ar, XRD characterizations were carried out on the calcined and reduced catalysts. Fig. 2 shows the XRD patterns of the calcined and reduced catalysts. As can be seen from Fig. 2A, except for the Cu7Ni/HMS sample, no obvious diffraction peak attributed to copper and nickel species could be observed except a broad diffraction peak at 2θ around 22° coming from amorphous silica, which indicated that the copper and nickel species were highly dispersed on the silica support. When the nickel content was higher than 5 wt%, diffraction peaks at 35.5° and 38.7° assigned to CuO (JCPDS05-0661) could be observed, but no diffraction peaks attributed to nickel species could be detected, which suggests that the introduction of the proper amount of nickel species could not affect the dispersion of copper species and the existence of copper species might enhance the dispersion of nickel species. The formation of nickel phyllosilicate might be another factor in the highly dispersed nickel species, which is in accord with the result reported by Burattin et al. [37].

Fig. 2B presents the XRD patterns of the reduced catalysts. For 3Ni/HMS-re catalyst, distinct diffraction peaks at 37° and 44.3° assigned to the NiO phase (JCPDS78-0643) could be observed. In addition, nickel silicate species could be observed, which indicated that redissolution and reprecipitation might occur to form silicate. Because of the high resistance to sintering of the nickel oxide particles before reduction and the metal particles during reduction, the average metal particle size calculated from the Scherrer equation is 7.2 nm [37]. For nickel-modified Cu/HMS samples, two obvious diffraction peaks at 37° and 44.3° attributed to NiO and Ni or Cu, respectively, could be observed and no detectable silicate species could be found, which indicated that the interaction between metallic (Cu and Ni) species and silica was affected by the amount of nickel. It is worth noting that the 2θ values of NiO, metallic Cu, and Ni are almost the same; thus it is difficult to distinguish among NiO, Cu, and Ni at $2\theta = 44.3°$. Moreover, a copper and nickel oxide solid solution might be formed due to the similar *fcc* structures with similar lattice parameters. As a conclusion, the reduced catalysts are composed of metallic Cu species, NiO species, or metallic nickel species.

3.1.2. Redox properties of the catalysts

The reducibility of the complex oxides revealed the intimate metal–support interaction in these compounds. Fig. 3 shows the H_2-TPR profiles of the series of calcined samples. For the 3Ni/

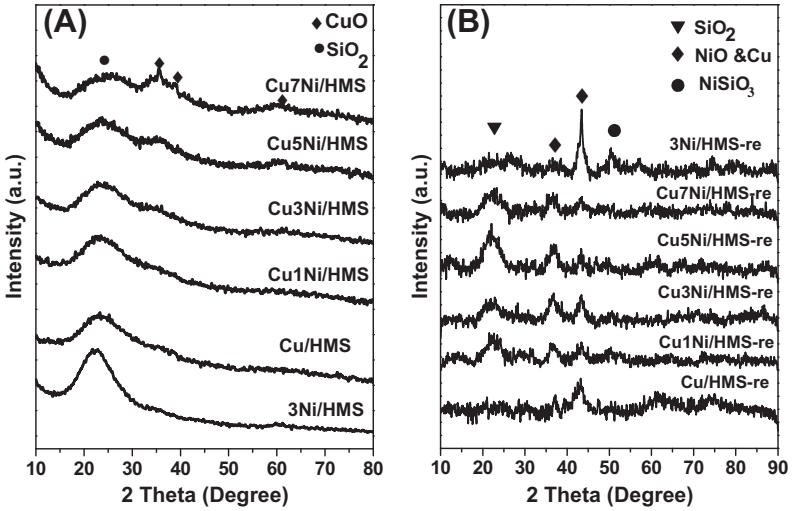

Fig. 2. XRD patterns of catalysts modified with different nickel amounts: (A) after calcination; (B) after reduction with 5% H_2/Ar at 573 K for 4 h.

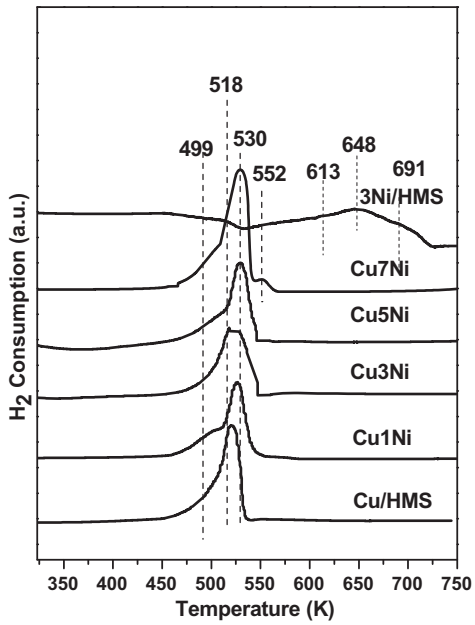

Fig. 3. TPR profiles of catalysts modified with different nickel amounts.

HMS sample, the temperature at which the maximum reduction peak (648 K) is substantially lower than that for the reduction of unsupported pristine NiO (703 K) [38]. This phenomenon illustrated that there was interaction between the nickel species and the silica support. After deconvolution of the peaks contained in the envelope of the TPR pattern and taking into account the nickel phyllosilicate and the nickel species that strongly or weakly interacted with silica, the wide reduction peak could be divided into three parts: nickel phyllosiliacate, highly dispersed nickel species with stronger interaction with the support, and bulk nickel species with weak interaction with the support, positioned at 613, 648, and 691 K, respectively.

For catalysts modified with different amounts of nickel, besides the main reduction peak at 530 K, there was a shoulder peak at ca. 499 K, which was attenuated for the Cu3Ni/HMS sample, and became more obvious at higher or lower nickel contents. The broad reduction peak indicated strong interaction between the metals, which might form a solid solution. It is known that the radius of Ni^{2+} is smaller than that of Cu^{2+}, and the eventual incorporation of Ni^{2+} into the CuO framework causes a slight contraction of the lattice. By comparison with the reference data for 3Ni/HMS and Cu/HMS samples, the feature at 530 K is attributed to the reduction of the copper oxides to metallic copper, while the peak at higher temperature is assigned to the reduction of nickel oxide. The presence of nickel shifts the reduction peak positions of copper species and the presence of copper also alters those of nickel species. Naghash et al. [38] also observed CuO reduction at low temperature in $CuNi/Al_2O_3$ catalysts. Bridier and Perez-Ramirez [39] observed the same phenomena on the Cu–Ni–Fe catalyst. In addition, the maximum reduction temperature of nickel species was greatly decreased (even lower than 570 K) due to the existence of copper, which was in good agreement with the results in the literature [38].

The reduction of NiO is also catalyzed by metallic copper [38], as pure nickel oxide is typically reduced at above 700 K. On the other hand, the maximum reduction temperature of copper was increased from 518 to 530 K by the introduction of nickel, which might result from the interaction between copper and nickel. Based on the XRD characterizations, the lowest reduction temperature (499 K) could be attributed to the reduction of highly dispersed copper species, the mediated reduction temperature (518 K) could be attributed to the reduction of copper species surrounded by Si or Ni species (through O^{2-} linkage), and the highest reduction temperature (530 K) might originate from the reduction of copper and nickel oxide solid solutions. By deconvolution of the H_2 consumption peak, it could be found that the proportion of the higher reduction species increased as the increase of the nickel contents. For the Cu7Ni/HMS sample, an additional reduction peak appeared at ca. 552 K, which could be attributed to the reduction of bulk NiO.

Based on the XRD results, we know that the Ni content has a strong influence on the stabilization of the copper nanoparticles. No obvious diffraction peaks assigned to CuO could be observed except for the Cu7Ni/HMS sample, which indicated that the introduction of nickel species could hinder the aggregation of copper species by increasing the surface area through forming nickel phyllosilicates. After reduction, the copper species dispersed homogeneously on the surface of the support. Thus, the exposed metallic Cu surface area could be greatly improved from 11.6 to 21.6 $m^2\ g^{-1}$. Combined with the relevant characterizations, a schematic model of the structure evolution of the copper species with the increasing of the nickel loading is given in Scheme 1. Without the introduction of the nickel species, the copper species was highly dispersed on the surface of the silica support. However, it was easy to aggregate during the reaction due to the weak interaction between copper and silica support. After modification with 1 wt% Ni, two kinds of copper species appeared, highly dispersed copper and segregated copper clusters. With further increased nickel content, an optimized dispersion of copper species could be obtained. In addition, the interaction between the copper species, the silica support and the interface in the support, the copper species, and the nickel species could be further enhanced via the highly dispersed nickel species. However, excess introduction of nickel would lead to the aggregation of part of the nickel oxide, which blocked the active copper sites.

3.1.3. Surface chemical states of the catalysts

The use of XPS intensity ratios of metal catalysts to the support provides information regarding the dispersion degree of the active metal on the support. The results of the XPS intensity ratios of M/Si (M = Cu, Ni) as a function of nickel content are presented in Fig. 4. As shown in Fig. 4A, the surface content of copper increased with increased amount of nickel, indicating that the introduction of nickel species was beneficial for the surface enrichment of copper species. The surface Cu/Si ratio exhibited exponential growth with the increase of nickel content over the calcined samples, especially when the nickel content was higher than 3 wt%, which suggested that the copper species were easier to segregate on the surface of the sample after calcination. After reduction, however, the surface content of copper species obviously decreased in comparison with that of the calcined samples and the surface Cu/Si ratio was almost proportional to the nickel content, which meant that the pretreatment of H_2 could alter the surface distribution of copper and nickel

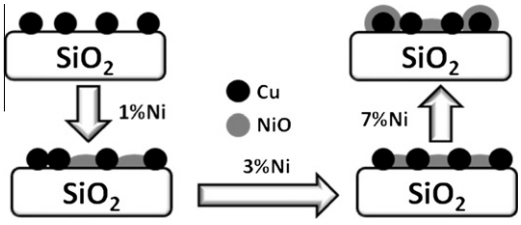

Scheme 1. Schematic model for the variation of Cu species with increased nickel content.

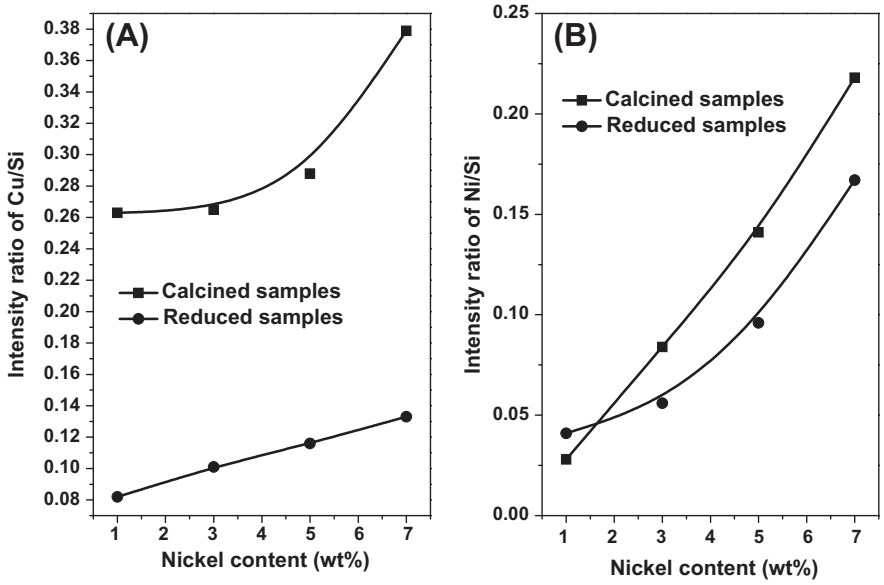

Fig. 4. Intensity ratios of M/Si based on XPS results: (A) Cu/Si ratios before or after reduction; (B) Ni/Si ratios before or after reduction.

species. Different from that for $CuNi/SiO_2$ samples, the surface Cu/Si ratio could be enhanced on the Cu/SiO_2 sample after being reduced with H_2 [29]. In addition, the surface nickel content (Fig. 4B) of the reduced samples was also lower than that of the calcined samples. To further elucidate the distributions of the surface metals, the bulk and surface Ni/Cu ratios in the calcined and reduced samples as a function of nickel content are presented in Fig. 5. The surface Ni/Cu ratios, especially in the reduced samples, were much higher than those of the bulk, which indicates that the surface enrichment of nickel occurred after the introduction of nickel. The enrichment of nickel became more obvious when the samples with higher nickel content (more than 3 wt%) were pretreated under a reducing atmosphere. It might be the nickel enrichment on the surface that greatly improved the dispersion of the copper species, tremendously enhancing the catalytic hydrogenation performance.

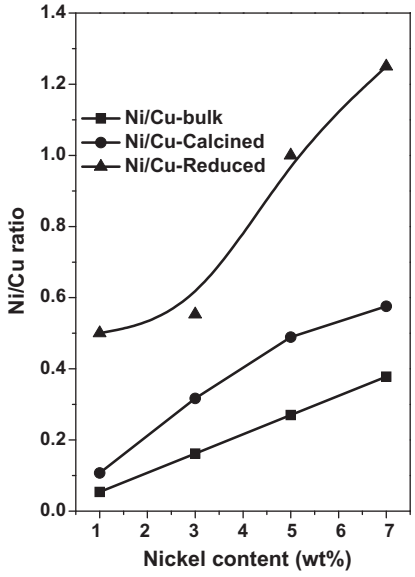

Fig. 5. Surface intensity ratios of Cu/Ni based on XPS results and bulk intensity ratios of Cu/Ni.

Fig. 6 shows the Cu2*p* XPS spectra of the calcined and reduced samples. Typically, the $Cu2p_{3/2}$ BE of CuO is found at ca. 933.5 eV [40], and this value of the supported copper phyllosilicate is 934.9 eV [41]. Fig. 6A shows that the copper in all the calcined samples existed in the oxidation state of Cu^{2+}, as evidenced by the $Cu2p_{3/2}$ peak at 933–936 eV and the 2*p* to 3*d* satellite at 942–945 eV characteristic of Cu^{2+} with electron configuration of $3d^9$ [42]. The intensities of the shake-up lines relative to the main core level of both the $Cu2p_{3/2}$ and $2p_{1/2}$ levels varied as a function of nickel content. The shake-up intensities denoting oxidative copper species on the surface were relatively more intense at higher nickel content. The variation of the $Cu2p_{3/2}$ BE values with the nickel content is an indication of the formation of different copper species in the calcined samples. The peak fitting of the $Cu2p_{3/2}$ core level spectra revealed two BE states at 934.4 and 936.0 eV, which were assigned to the copper species interacted with silica and nickel, respectively. The XPS spectra of the reduced samples are illustrated in Fig. 6B. Compared with the calcined samples, the $Cu2p_{3/2}$ BE of the reduced catalysts was shifted to ca. 932.7 eV, and the 2*p* to 3*d* satellite disappeared due to the reduction of Cu^{2+} to Cu^0 and/or Cu^+. Besides, the BE of $Cu2p_{3/2}$ shifted to lower values with increased the nickel content, indicating the electronic effect was more obvious as the nickel content increase.

Fig. 7 shows the Ni2*p* XPS spectra of the calcined and reduced catalysts. Fig. 7A shows that all the calcined samples exhibited a main peak with a satellite at higher BE. For divalent nickel compounds, the main peak corresponded to the final state of $2p^5 3d^9 L$ (L means a ligand hole) and the satellite peak to a $2p^5 3d^8$ final state. Compared with the bulk Ni 2*p*3/2 (854.9 eV), the main peak of the calcined samples appeared at higher BE, which indicated the much stronger interaction between the nickel species and the silica support. In addition, the spectrum of the main peak showed two overlapped peaks at low (857.6 eV) and high (858.9 eV) BE values, which could account for the changes in linking arrangements of Ni cations within the lattice in the composite catalyst. Thus Ni^{2+} ions surrounded by Cu^{2+}(through O^{2-} linkage) as second neighbors showed a much higher BE than isolated Ni^{2+} ions surrounded by other Ni^{2+} cations. Shape changes in XPS spectra were observed with the increase of the nickel content, suggesting that nickel is in different valence states as the amount increases. After reduction, the BE value of the nickel species decreased compared with that in

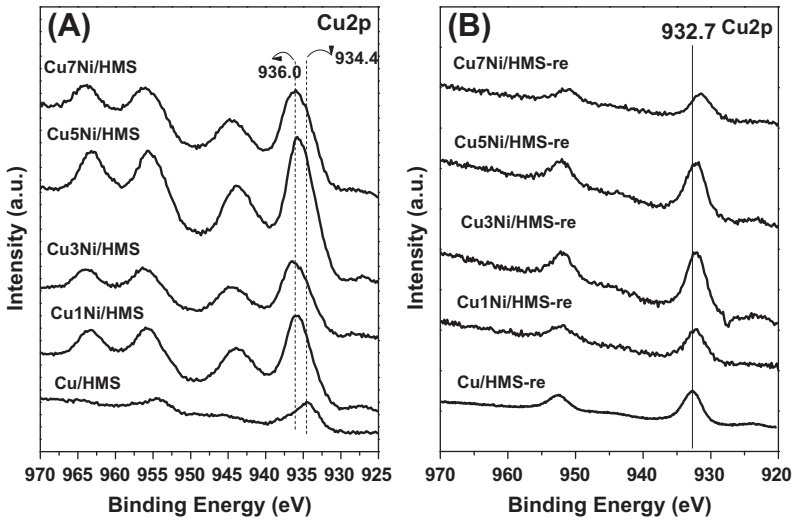

Fig. 6. Cu2*p* photoelectron spectra of catalysts modified with different nickel amounts: (A) after calcination; (B) after reduction.

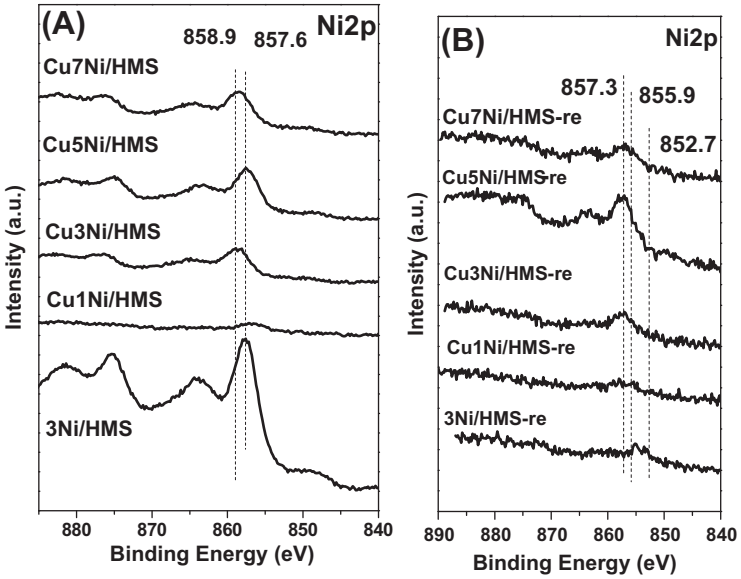

Fig. 7. Ni2*p* photoelectron spectra of catalysts modified with different nickel amounts: (A) after calcination; (B) after reduction.

the calcined samples. No characteristic peak with BE 852.7 eV, attributed to the metallic nickel species, could be observed, implying that all the nickel species exhibited oxidized chemical states on the surface of the catalysts.

To investigate the surface Cu and Ni chemical environments of the catalysts during the reaction, the XPS spectra of Ni2*p* and Cu2*p* for the postcatalyst of Cu3Ni/HMS was also performed (see the supporting information). It was found that no obvious differences in the BE values and surface ratios of Cu/Si, Ni/Si, and Ni/Cu could be observed, which indicated that the surface chemical states and surface chemical compositions of the Cu3Ni/HMS catalyst were relatively stable during the whole reaction.

The evolution of the different electronic parameters of copper and nickel with the amount of the nickel content can be observed in Fig. 8. As in the previously described experiment for the calcined and reduced samples, most of the changes in the BE occurred for relatively low content of nickel species. The difference in BE values among samples with different nickel content indicated that the electron transfer between copper and nickel species could happen during the catalyst calcination and the reduction processes.

3.2. Characterization of bimetallic CuNi samples

3.2.1. Structural evolution of the catalysts

To investigate the effect of metallic nickel on catalytic performance, different bimetallic CuNi/HMS catalysts were also prepared by the chemical reduction deposition method. Fig. 9 shows the XRD patterns of bimetallic catalysts with different Cu/Ni molar ratios. As a comparison, the XRD pattern of the reduced Cu/HMS sample is also presented in Fig. 9. No obvious diffraction peaks except the one at $2\theta = 22^\circ$ could be observed for most of the samples, indicating that all the bimetallic species were highly dispersed. However, for Cu_3Ni_1/HMS, two peaks positioned at $2\theta = 43.9^\circ$ and 51.9° were observed, which corresponded to the (1 1 1) and (2 0 0) lattice of the Cu, Ni, or Cu–Ni alloy. Since Cu and Ni have the same *fcc* structure and almost the same lattice constant, we cannot distinguish copper–nickel alloy from a mixture of the monometallic phases from the XRD patterns alone. However, according to the literature results [38], we believe that nanoparticles of Cu–Ni alloy were formed after the reduction pretreatment. In combination with the TPR results, the XRD peaks presented here

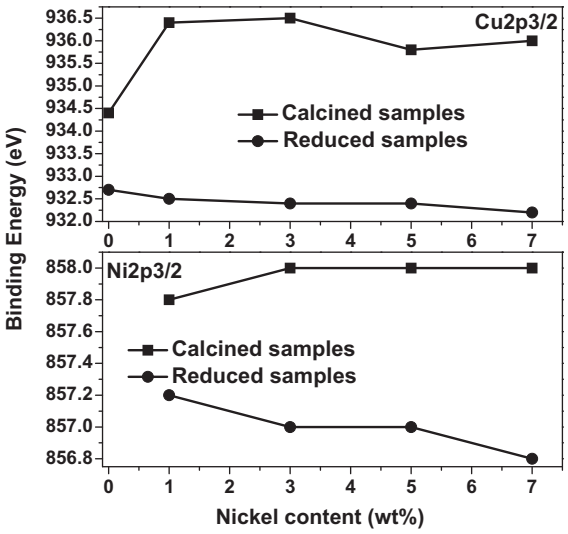

Fig. 8. Evolution of the Cu2$p_{3/2}$ and Ni2$p_{3/2}$ BEs for increasing nickel amounts.

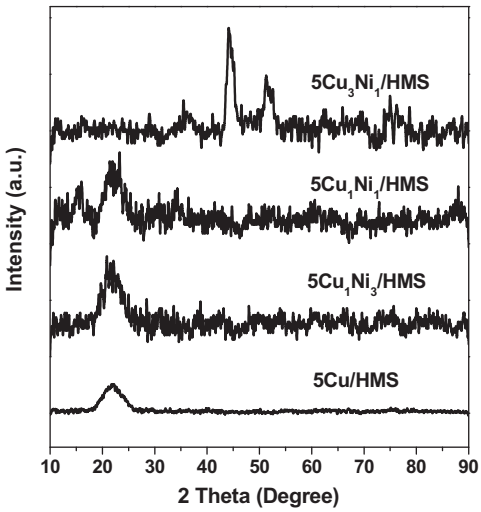

Fig. 9. XRD patterns of bimetallic catalysts with different molar ratios of Cu/Ni. [Comp: change horizontal axis label from 2θ (°) to 2θ (°)].

should be ascribed to alloys of Cu–Ni or metallic Cu or Ni. One can see that the XRD peaks become more obvious with increasing copper content in the samples. Using the Scherrer equation, the particle size calculated from the peak width of the (1 1 1) reflection for Cu_3Ni_1/HMS is estimated as 8.4 nm. It is clear that the particle size of the Cu–Ni alloy becomes smaller with increasing Ni content, which is also confirmed by the TEM observations.

Fig. 10 shows a typical TEM image for a CuNi/HMS sample with an atomic ratio Cu/Ni = 1:1. One can see that the metal particles are uniformly dispersed throughout the support and show a narrow particle-size distribution with an average particle size of 2.7 ± 0.5 nm (not shown here). Fig. 10 also (on the right) shows the EDX of the sample with Cu/Ni ratio 1/1, demonstrating the coexistence of Cu and Ni. The Cu/Ni ratio is measured to be 50.7/49.3, which is in excellent agreement with the initial ratio as added.

3.2.2. Redox properties of the catalysts

To further elucidate the interaction between copper and nickel species and the distribution behavior of the bimetallic species, TPR characterizations were carried out for the bimetallic samples pretreated under air. After pretreatment at 673 K under static air, the alloy samples could be oxidized homogeneously and a uniform solid solution was formed; thus, under the reduced conditions, one symmetric hydrogen consumption peak can be observed. Fig. 11 shows the TPR results of the oxidized alloy samples. For comparison, the monometallic supported HMS samples were also evaluated. The reduction temperature of the nickel-supported sample (920 K) is substantially higher than that of the copper-supported one (530 K), which indicates that the copper species were reduced more readily than nickel species. After the introduction of copper, the higher reduction peak disappeared and a lower symmetry peak was observed at a relatively lower reduction temperature, implying that the two metallic species were homogeneously mixed. With increased nickel content, the reduction peak temperature decreased, showing that the copper species could remarkably enhance the reducibility of the mixed oxide catalysts. However, the separated reduction peaks appeared at lower temperature and higher temperature at the same time when the molar ratio of Cu/Ni reached 1/3, indicating almost no interaction between copper and nickel species. In other words, the copper or nickel species are distributed on the support separately or as clusters. Differences in peak temperatures between Cu_1Ni_1/HMS and Cu_3Ni_1/HMS samples might result from the different interaction between copper and nickel species. By adjusting the Cu/Ni molar ratio, different bimetal samples could be obtained.

3.2.3. Surface chemical states of the catalysts

Fig. 12 shows the Cu2p and Ni2p XPS spectra of the bimetallic catalysts. The BE of Cu2$p_{3/2}$ core levels was in the range 932.2–

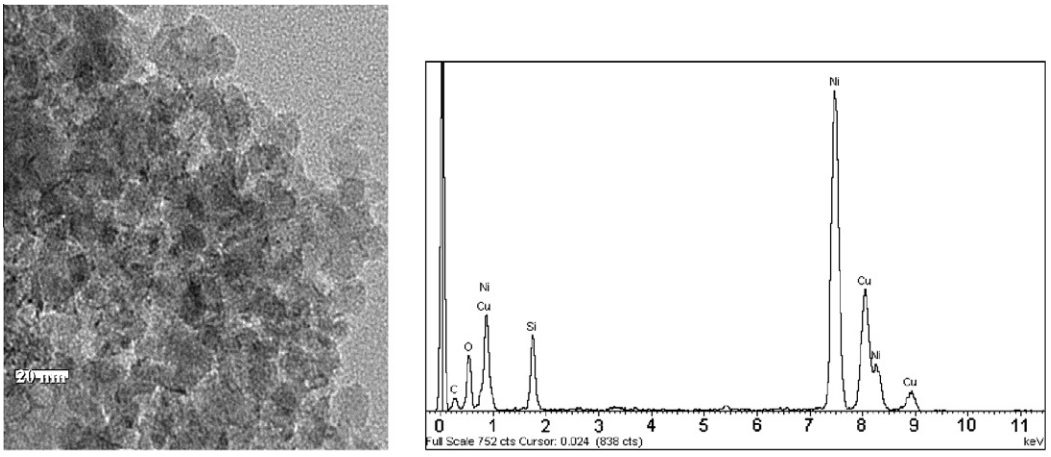

Fig. 10. TEM image of bimetallic Cu_1Ni_1/HMS sample and EDX analysis of individual particles.

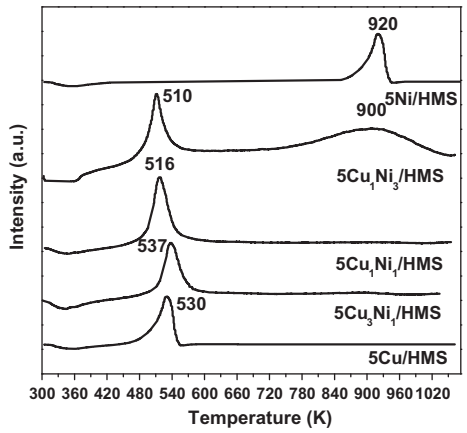

Fig. 11. TPR profiles of bimetallic catalysts with different ratios of Cu/Ni.

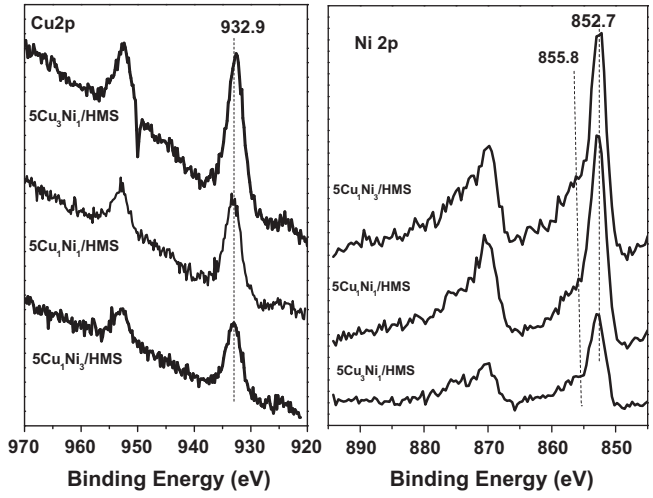

Fig. 12. XPS spectra of bimetallic catalysts: (A) Cu2$p_{3/2}$; (B) Ni2$p_{3/2}$.

932.6 eV, indicating that metallic copper existed on the surface of the catalysts. The difference in BE might originate from the different electronic interactions between copper and nickel species. In addition, the BE of Ni2$p_{3/2}$ was mainly at 852.7 eV, with a shoulder peak in a higher band, which might result from the partial oxidation of nickel species during the operation. On the basis of the XPS characterization results, the chemical states of the copper and nickel species were both metallic. It was worth noting that no obvious difference could be observed in BE for either metal as a function of bimetallic composition. However, compared to the reduced monometallic Cu and Ni catalysts, an obvious difference in BE for either metal could be observed. For reduced monometallic Cu/HMS, the BE of Cu is 932.6 eV, while for bimetallic CuNi/HMS, the BE of Cu is 932.8 eV; for reduced monometallic Ni/HMS, the BE of Cu is 855.9 eV, while for bimetallic CuNi/HMS, the BE of Ni is 852.7 eV. The increase in BE of Cu and the reduction in BE of Ni for bimetallic CuNi/HMS compared to the monometallic catalyst might be related to changes in unfilled *d*-band electron holes arising from the charge transfer from Cu to the adjacent Ni.

Characterization of the chemical state of an element on a support by XPS has traditionally been carried out by comparing their BEs with those of the bulk. For example, for copper or copper oxide supported phases, BE changes have also been attributed to the size of the deposited metals or oxides. Several reasons for BE changes have been invoked: variation of the average coordination number of particle atoms due to a high surface-to-volume ratio, decrease in the electron density of supported particles with respect to the bulk metal or oxide, and alloying and/or chemical interaction with the support. Similar changes in the electronic characteristics of oxide particles and layers deposited on the substrates of other metal oxides were also attributed to the dispersion degree of the deposited phase (assuming this decrease in the amount of deposited material). The linking arrangement of nickel in the solid solution with other nickel or silica cations accounted for the large changes in BEs at the high end of the spectra.

3.3. Catalytic activity and stability

3.3.1. Effect of NiO loading on the catalytic performance of DMO hydrogenation

DMO hydrogenation reaction was carried out to study the catalytic properties of NiO-modified Cu/HMS catalysts, and the conversion and selectivity as a function of LHSV are shown in Fig. 13. Because of the much higher dispersion of copper species and the promotion effect of nickel oxide, the nickel oxide modified catalysts presented much better catalytic performance than Cu/HMS in the hydrogenation of DMO. Even at a LHSV of 1.0 h^{-1}, which is significantly higher than those reported in the literature [28–31], nickel-modified Cu/HMS with nickel content of 3 wt% showed 100% conversion for DMO hydrogenation with 98% selectivity to EG. Nevertheless, only 88% of DMO conversion with an obviously low selectivity (34%) toward EG was obtained over Cu/HMS catalyst at the same LHSV. In addition, almost no conversion could be detectable over Ni/HMS catalyst. All these results indicated a synergetic effect over the nickel-modified copper catalysts and the high efficiency of the nickel–copper containing catalysts in DMO hydrogenation. Along with the increase of the nickel content, the yield of EG exhibited a volcanic variation trend, and the highest yield could be obtained over the catalyst with Ni content of 3 wt%. The reason for the significant decrease in catalytic performance over catalysts with nickel content higher than 3 wt% as compared to the Cu/HMS catalyst most probably originates from the dramatic decrease of active sites on the surface due to the segregation of nickel oxide on the surface, which blocks the active copper species. Compared with literature reports [28,31], the nickel-modified catalyst exhibited much higher reaction activity than the catalysts prepared by impregnation and ion exchange.

As we know, Cu/SiO_2 catalyst has been widely applied in many gas-phase hydrogenation reactions, such as hydrogenation of dimethyl maleate to 1,4-butanediol [43], hydrogenation of glycerol to 1,2-propanediol [44], and selective hydrogenation of cinnamaldehyde [45]. The metallic Cu surface area at the same active site was compared. It was found that the nickel-modified catalyst exhibited much higher Cu surface area than the above-mentioned catalysts.

3.3.2. Effect of composition of bimetallic CuNi on the catalytic hydrogenation of DMO

Based on the characterizations of the nickel-modified catalysts, the surface chemical state of nickel is not metallic but oxidative. The oxidative nickel species played an important role in improving the activity in the hydrogenation of DMO and the selectivity to EG. To further elucidate the role of chemical states of nickel in catalytic performance, bimetallic CuNi catalysts were prepared by the chemical reduction deposition method. Interestingly, MG, the first-step hydrogenation product, was the main product over the bimetallic catalysts. This finding was totally different from those for the monometallic copper catalysts. The catalytic performance over different bimetallic catalysts is summarized in Table 2. Under the reaction conditions specified in the caption of Table 2, up to 96% selectivity to MG with 86% conversion of DMO could be obtained over the bimetallic catalyst with Cu/Ni ratio 1:1. Although

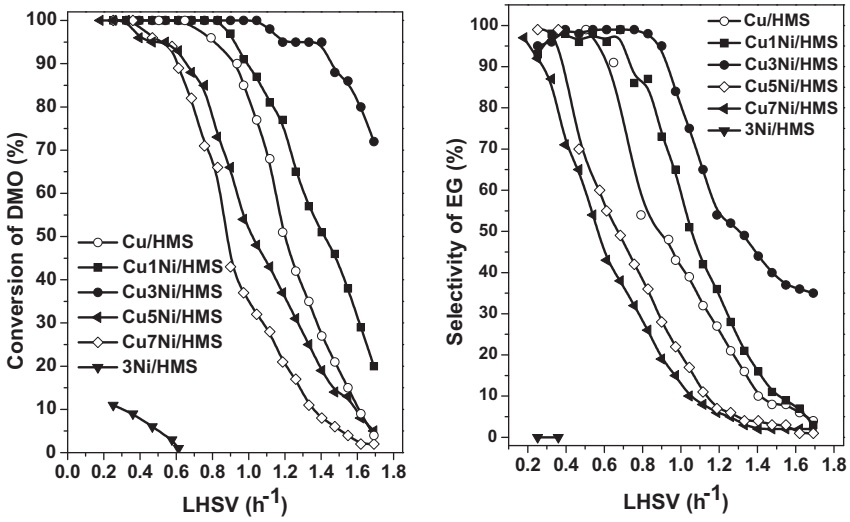

Fig. 13. Effect of the LHSV of DMO on the catalytic performance of the nickel-modified catalysts. Reaction conditions: 2.5 MPa H_2, 473 K, and H_2/DMO ratio 100 (mol/mol).

Table 2
The catalytic performance of bimetallic catalysts with different ratios of Cu/Ni in gas-phase hydrogenation of DMO[a].

Catalyst	T (K)	C_{DMO} (%)	S_{MG}	S_{EG} (%)	S_{Cu}[b] ($m^2\ g_{Catal}^{-1}$)	TOF[c] (h^{-1})
Cu_3Ni_1/HMS	493	89	60	40	8.2	7.0
Cu_1Ni_1/HMS	493	100	86	14	6.1	10.6
Cu_1Ni_3/HMS	493	27	67	33	3.6	4.8
Cu/HMS	493	88	14	86	11.6	4.9
Ni/HMS	493	0	0	0	–	–

[a] Reaction condition: 2.5 MPa, H_2/DMO ~ 100 (mol/mol), and LHSV of DMO 0.2 h^{-1}.
[b] Cu metal surface area determined by N_2O titration method.
[c] Turnover frequency (DMO molecular reacted per mol surface Cu per hour) at LHSV = 0.2 h^{-1} at 493 K.

the conversion of DMO could be improved with higher reaction temperature, the selectivity to MG would decrease, accompanied by a corresponding increase in the selectivity to EG. The bimetallic composition was found to have a strong influence on the catalytic performance in the hydrogenation of DMO. Excessive introduction of nickel or copper would greatly decrease the activity of the catalyst, which indicated that the proper surface composition was necessary to obtain high DMO conversion and MG selectivity.

In the literature reports on bimetallic Ni–Cu systems, surface segregation of Cu is predominantly reported [46], justified on the basis of thermodynamics. Because of the lower heat of sublimation (i.e., lower surface free energy) of Cu compared with Ni, Cu is prone to occupy the surface sites of the bimetallic particles [46]. However, surface segregation of Ni has been reported in polymer supported NiCu nanoparticles [47] and has also been observed by in situ TEM over Ni–Cu/TiO_2 [48]. In the present work, Ni and Cu were uniformly distributed within the particle when the Cu/Ni ratio was higher than 1:1, indicating the formation of homogeneous Ni–Cu solid solution nanoparticles. The synergetic effects generated by the Ni–Cu solid solution greatly changed the reaction dynamics, which made MG the main product. The selectivity to MG depends critically on the Cu/Ni ratio; higher nickel content leads to decreased selectivity and DMO conversion. It has been reported that the bimetallic surface structure including bimetallic composition, the binding energy, and the bonding morphologies played a crucial role in selective hydrogenation reactions especially for C=O and C=C hydrogenation [49–51]. The presence of 3*d* transitional metal on the surface or subsurface due to different binding energies and bonding morphologies with the adsorbed substrate has a strong influence on the selectivity of the unsaturated aldehyde hydrogenation. The great difference in selectivity for hydrogenation of DMO might be due to the different surface structures mentioned above, modified with transitional metal or oxide on the surface or subsurface of the catalyst. Phase segregation is observed when the Cu/Ni ratio reaches 1/3, and Ni bleeds out from CuNi and the Cu content in the remaining nanoparticle increases accordingly. This phenomenon can be explained by the following considerations. (1) The reduction of the Cu precursor is faster than that of the Ni precursor. Therefore, it is easier and quicker to form reduced Cu-containing species in the early stage of the reduction process. (2) Cu and CuO have lower Tamman temperatures than Ni and NiO; thus on the silica surface, Cu species diffuse faster than Ni species, which leads to rapid formation of Cu crystals. (3) The slower diffusion of the Ni species to the Cu-rich nuclei leads to the formation of particles with a Cu-rich core and Ni-rich shell. Because of the Ni segregation on the surface of the Cu species, the number of active sites greatly decreased; thus the catalytic hydrogenation activity was reduced compared with that of the homogenous bimetallic Cu–Ni samples.

It is well known to us that monometallic Ni is active in many hydrogenation reactions such as CO_2 hydrogenation [52], liquid phase citral hydrogenation [53], and hydrogenation of *o*-, *m*-, and *p*-xylene [54] due to its strong ability to dissociate hydrogen and adsorb C=O. However, monometallic Ni is not active in the hydrogenation of DMO, which might result from the strong dimethyl oxalate adsorption on the surface of Ni, which poisons the surface. If metallic Cu exists on the surface of catalysts such as CuNi/HMS, on one hand, it could dissociate hydrogen molecules to hydrogen atoms; on the other hand, it could react with adsorbed DMO molecules to form the product. As for EG or MG, this might depend on the adsorption morphology of DMO. If Ni adsorbs only one C=O bond, then MG will be obtained; however, if Ni adsorbs two C=O bonds, then EG will be obtained. As for the concrete adsorption, it is beyond our research in the present work.

Various mechanisms can be considered in which the nickel species influence the catalytic properties of the deposited metal. Another possibility would be direct participation of the support material in the catalytic reaction. The special active sites might form at the metal–support perimeter, which might be able to coordinate and activate different functional groups in the DMO molecule. As described in the Experimental section, the Cu–Ni bimetallic catalysts could be formed homogeneously by tuning the Cu/Ni ratio. XPS results showed that when nickel was dispersed

in copper, changes in the electronic properties of nickel resulted in the displacement of BEs to lower values, depending on the copper content. The change of the electrical properties might lead to a change in the catalytic behavior.

The quantitative evaluation of each factor with respect to electronic variations between the Ni and Cu or Ni and Si can be done by comparing the BE value changes with the quantum–mechanical bond structure of M–O–Si at the interface. This information and a quantum–mechanical description of M–O–Si bonds at the interfaces in terms of covalence, and also the density of charge distribution, would be necessary to completely illustrate the observed changes.

3.3.3. Effect of Ni chemical state on the catalytic behavior for hydrogenation of DMO

Hydrogenation of DMO to EG via MG is a two-step continuous hydrogenation process. From the thermodynamic point of view, it is inclined to generate EG due to the much higher equilibrium constant of the second step than that of the first one. Therefore, high EG selectivity could be obtained in the context of high hydrogenation conversion. Our previous studies showed that silica-supported copper catalysts with highly dispersed active copper species exhibited high efficiency in the synthesis of EG from the hydrogenation of DMO [29]. Thus, highly efficient catalysts could be designed to have higher dispersion of copper species and much stronger interaction between the active sites and the support. Introduction of aluminum into the silica support provided both greater copper dispersion and stronger interaction with the support; however, acid sites were also generated, which was favorable to the dehydration reaction [33]. How to design a highly efficient catalyst without generating acidity is still a great challenge, which lies in the dynamical control of the product distribution, and could be achieved by nanocasting highly active and chemoselective catalysts.

By introducing nickel species through different synthetic procedures, several copper catalysts modified with nickel species having different surface chemical states were prepared and exhibited high conversion and chemoselectivity. The introduced amount of nickel species was found to have a profound effect on the chemoselectivity of the hydrogenation of the DMO reaction. To establish the real effect of Ni loading on EG selectivity for CuxNi/HMS series, S_{EG} was compared at the same DMO conversion (about 50%) and listed in Table 1. As can be seen from Table 1, the EG selectivity is a function of Ni loading at the same DMO conversion at ~50%. The maximum EG selectivity could be obtained via the Cu3Ni/HMS catalyst, which indicates that the Ni content indeed had a great influence on the selectivity of EG. By using AE, oxidative nickel-modified Cu/SiO_2 catalyst could be obtained and exhibited excellent catalytic performance in the synthesis of EG. A 100% DMO conversion and 98% selectivity to EG could be obtained at LHSV 1.0 h^{-1} over Cu3Ni/HMS catalyst. Using the chemical reduction deposition method, a bimetallic catalyst was prepared and also exhibited good catalytic hydrogenation performance in the synthesis of MG, which was completely different from that of the oxidative nickel-modified catalyst. By adjusting the molar ratio of Cu to Ni, nearly 96% selectivity to MG with 86% conversion of DMO could be achieved. The great difference in catalytic behavior might lie in the different surface compositions induced by the nickel species.

3.3.4. Catalytic stability

The long-term stability of catalysts is important for gas-phase DMO hydrogenation to MG and EG from both academic and industrial viewpoints. To investigate the stability of the NiO-modified Cu/HMS catalyst, comparisons of catalytic activity and selectivity to EG as a function of reaction time for Cu3Ni/HMS and Cu/HMS catalysts are displayed in Fig. 14A. The Cu3Ni/HMS catalyst showed excellent performance in both catalytic activity and selectivity to EG, which was stable for 150 h. In contrast, obvious deactivation of nickel-free Cu/HMS catalyst was observed within 45 h under identical reaction conditions. To investigate the stability of the bimetallic CuNi/HMS catalyst, comparisons of catalytic activity and selectivity to MG as a function of reaction time for Cu_1Ni_1/HMS and Cu/HMS are shown in Fig. 14B. The Cu_1Ni_1/HMS catalyst exhibited outstanding catalytic performance, which was stable for 50 h. However, evident deactivation of the monometallic Cu/HMS catalyst could be observed within 12 h under identical reaction conditions. The stability of Cu3Ni/HMS and Cu_1Ni_1/HMS could be attributed to the stable surface chemical environments, including surface chemical compositions and surface species structures, which could be determined from the XPS results by comparing the chemical environments of the reduced catalysts and the postcatalyst. XPS characterizations were carried out for the postcatalyst by taking the following factors into consideration. First, the substrates (DMO, MG) are oxygenates, which are presumably adsorbed via the carbonyl oxygen atoms on the catalyst surfaces under working conditions. Second, methanol is not only the carrier that has been used to supply DMO (and MG) to the catalysts, but also a stoichiometric co-product of both reactions. Third, notwithstanding the strongly reducing reaction conditions used, the presence of these oxygenates on the surfaces of the working catalysts may result in significant changes in the Cu/Ni valence state distributions relative to those measured for the catalysts in the pristine

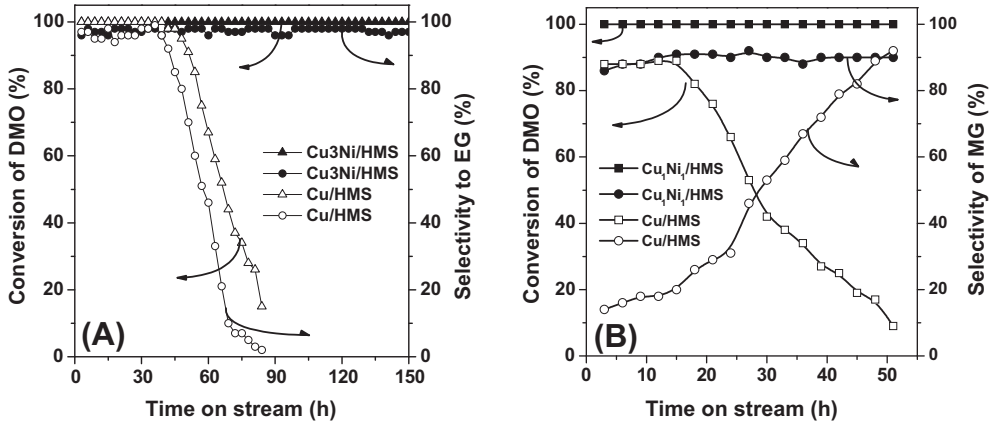

Fig. 14. Catalytic performance of catalysts as a function of reaction time (A) over the Cu3Ni/HMS and Cu/HMS catalysts; (B) over the Cu_1Ni_1/HMS and Cu/HMS catalysts. Reaction conditions: (A) 2.5 MPa H_2, 473 K, and H_2/DMO ratio 100 (mol/mol). LHSV = 1.0 h^{-1}; (B) 2.5 MPa H_2, 493 K, and H_2/DMO ratio 100 (mol/mol). LHSV = 0.2 h^{-1}.

state, i.e., immediately after reduction but prior to exposure to the substrates, which is particularly relevant in view of the well-known extreme sensitivity of metallic Ni to oxidation. As can be seen from the spectra (see the supporting information), no obvious differences in the BE values and surface ratios of Ni/Cu, Cu/Si, and Ni/Si from the reduced catalysts could be observed, which indicated that the surface chemical state and surface chemical composition of the Cu3Ni/HMS and Cu_1Ni_1/HMS catalysts were relatively stable during the whole reaction. It was the stable surface chemical environments that made sure that good activity and selectivity could be maintained in the long term.

4. Conclusions

High yields of MG and EG could be achieved over nickel–modified copper catalysts by tuning the nickel surface chemical states. An 86% yield of MG and a 98% yield of EG could be obtained over Cu_1Ni_1/HMS and Cu3Ni/HMS, respectively. The chemical states of the nickel species were found to have a great influence on the catalytic behavior. Copper-based catalysts promoted by oxidative nickel species were favorable for EG synthesis due to the enhanced dispersion of copper species, while MG could be obtained chemoselectively over the bimetallic CuNi catalyst, which might result from the synergetic effects of the metallic copper and nickel species.

Acknowledgments

We thank the Major State Basic Resource Development Program (Grant 2003CB 615807), the NNSFC (Project 20973042), the Research Fund for the Doctoral Program of Higher Education (20090071110011) and the Science and Technology Commission of Shanghai Municipality (08DZ2270500) for financial support. Also, we express our sincere gratitude to one of the reviewers for important and constructive suggestions.

Appendix A. Supplementary material

Supplementary data associated with this article can be found, in the online version, at doi:10.1016/j.jcat.2011.03.006.

References

[1] C. Burda, X.B. Chen, R. Narayanan, M.A. El-Sayed, Chem. Rev. 105 (2005) 1025.
[2] A. Hugon, L. Delannoy, J.M. Krafft, C. Louis, J. Phys. Chem. C 114 (2010) 10823.
[3] C. Della Pina, E. Falletta, M. Rossi, J. Catal. 260 (2008) 384.
[4] J.A. Rodriguez, D.W. Goodman, Science 257 (1992) 897.
[5] T. Bligaard, J.K. Nørskov, J. Rossmeisl, C.H. Christensen, Nat. Chem. 1 (2009) 37.
[6] J.K. Nørskov, C.H. Christensen, Science 312 (2006) 1322.
[7] J.K. Nørskov, Nature 414 (2001) 405.
[8] F. Besenbacher, I. Chorkendorff, B.S. Clausen, B. Hammer, A.M. Molenbroek, J.K. Nørskov, I. Stensgaard, Science 279 (1998) 1913.
[9] A. Cao, G. Veser, Nat. Mater. 9 (2010) 75.
[10] A.Q. Wang, C.M. Chang, C.Y. Mou, J. Phys. Chem. B 109 (2005) 18860.
[11] X.Y. Liu, A.Q. Wang, X.F. Yang, T. Zhang, C.Y. Mou, D.S. Su, J. Li, Chem. Mater. 21 (2009) 410.
[12] P. Strasser, S. Koha, J. Greeley, Phys. Chem. Chem. Phys. 10 (2008) 3670.
[13] J.C. Dellamorte, J. Lauterbach, M.A. Barteau, Catal. Today 2 (2007) 182.
[14] S. Kameoka, A.P. Tsai, Catal. Today 132 (2008) 1.
[15] M.T. Schaal, A.Y. Metcalf, J.H. Montoya, J.P. Wilkinson, C.C. Stork, C.T. Williams, J.R. Monnier, Catal. Today 123 (2007) 142.
[16] M. Kang, M.W. Song, T.W. Kim, Can. J. Chem. Eng. 80 (2002) 63.
[17] T. Huang, S. Jhao, Appl. Catal. A Gen. 302 (2006) 325.
[18] R.J. Best, W.W. Russel, J. Am. Chem. Soc. 76 (1954) 838.
[19] M.K. Gharpurey, P.H. Emmett, J. Phys. Chem. 65 (1961) 1182.
[20] Y. Liu, D.Z. Liu, Int. J. Hydrogen Energy 24 (1999) 351.
[21] Y. Li, J. Chen, L. Chang, Y. Qin, J. Catal. 178 (1998) 76.
[22] K.C. Khulbe, R.S. Mann, Catal. Rev. Sci. Eng. 24 (1982) 311.
[23] J.H. Sinfelt, J.L. Carter, D.J.C. Yates, J. Catal. 24 (1974) 28.
[24] Y. Sun, H. Wang, J.H. Shen, H.C. Liu, Z.M. Liu, Catal. Commun. 10 (2009) 678.
[25] A.Y. Yin, X.Y. Guo, W.L. Dai, K.N. Fan, Chem. Commun. 46 (2010) 4348.
[26] W.M.H. Sachtler, G.J.H. Dorgelo, R. Jongepier, J. Catal. 4 (1965) 100.
[27] S. Huffner, G.K. Werthein, J.H. Wernika, Phys. Rev. 138 (1973) 14511.
[28] A.Y. Yin, X.Y. Guo, W.L. Dai, H.X. Li, K.N. Fan, Appl. Catal. A Gen. 349 (2008) 91.
[29] A.Y. Yin, X.Y. Guo, W.L. Dai, K.N. Fan, J. Phys. Chem. C 113 (2009) 11003.
[30] A.Y. Yin, X.Y. Guo, W.L. Dai, K.N. Fan, Acta Chim. Sin. 67 (2009) 1731.
[31] A.Y. Yin, X.Y. Guo, W.L. Dai, K.N. Fan, ChemCatChem 2 (2010) 206.
[32] A.Y. Yin, X.Y. Guo, W.L. Dai, K.N. Fan, Appl. Catal. A Gen. 377 (2010) 128.
[33] A.Y. Yin, X.Y. Guo, W.L. Dai, K.N. Fan, J. Phys. Chem. C 114 (2010) 4348.
[34] P.T. Tanev, T.J. Pinnavaia, Science 267 (1995) 865.
[35] J.W. Evans, M.S. Wainwright, A.J. Bridgewater, D.J. Young, Appl. Catal. 7 (1983) 75.
[36] G.R. Rodolfo, R. Jorge, N. Ruben, L. Rosario, M. Florentino, Catal. Today 107–108 (2005) 926.
[37] P. Burattin, M. Che, C. Louis, J. Phys. Chem. B 104 (2000) 10482.
[38] A.R. Naghash, T.H. Etsell, S. Xu, Chem. Mater. 18 (2006) 2480.
[39] B. Bridier, J. Perez-Ramirez, J. Am. Chem. Soc. 132 (2010) 4321.
[40] A. Gervasini, M. Manzoli, G. Martra, A. Ponti, N. Ravasio, L. Sordelli, F. Zaccheria, J. Phys. Chem. B 110 (2006) 7851.
[41] C.J.G. van der Grift, P.A. Elberse, A. Mulder, J.W. Geus, Appl. Catal. 59 (1990) 275.
[42] F. Raimondi, K. Geissler, J. Wambach, A. Wokaun, Appl. Surf. Sci. 189 (2002) 59.
[43] L.F. Chen, P.J. Guo, Z.L. Jun, M.H. Qiao, W. Shen, H.L. Xu, K.N. Fan, Appl. Catal. A 356 (2009) 129.
[44] L. Huang, Y.L. Zhu, H.Y. Zheng, M.X. Du, Y.W. Li, Appl. Catal. A Gen. 349 (2008) 204.
[45] B.M. Reddy, G.M. Kumar, L. Ganesh, A. Khan, J. Mol. Catal. A Chem. 247 (2006) 80.
[46] J.H. Sinfelt, Acc. Chem. Soc. 10 (1977) 15.
[47] S. Wu, C. Zhu, W. Huang, Chin. J. Polym. Sci. 14 (1996) 76.
[48] P. Li, J. Liu, N. Nag, P.A. Crozier, J. Catal. 262 (2009) 73.
[49] L.E. Murillo, A.M. Goda, J.G. Chen, J. Am. Chem. Soc. 129 (2007) 7101.
[50] S. Laref, F. Delbecq, D. Loffreda, J. Catal. 265 (2009) 35.
[51] L.E. Murillo, C.A. Menning, J.G. Chen, J. Catal. 268 (2009) 335.
[52] G.D. Weatherbee, C.H. Bartholomew, J. Catal. 68 (1981) 67.
[53] U.K. Singh, M.A. Vannice, J. Catal. 199 (2001) 73.
[54] M.A. Keane, J. Catal. 166 (1997) 347.